Swept Volume Approach for the Characterization of Pumping Loss of Shrouded Meshed Cylindrical Gears

Michael J. Hurrell
Aerospace Engineer
HX5 Sierra, LLC/TFOME II
Cleveland, OH, USA

Irebert Delgado
Rotating and Drive Systems Branch
NASA
Cleveland, OH, USA

Jerzy T. Sawicki
Department of Mechanical Engineering
Cleveland State University
Cleveland, OH, USA

ABSTRACT

High speed rotorcraft transmissions are subject to load-independent power losses consisting of drag and pumping loss. Tightly conforming shrouds enclosing the transmission gears are often incorporated to reduce the drag component of the total load-independent losses. However, tightly conforming axial shrouding can result in an increase in the pumping loss component. Quantifying the pumping loss of shrouded gear transmissions has been the subject of many studies. This study presents a new approach for estimating pumping loss based on the concept of swept volume borrowed from the positive displacement pump and compressor industry. In this study, pumping loss of shrouded gear transmissions is considered to be related to the swept volume of the gear sets and the downstream flow resistance created by the shroud clearances. The drag loss and pumping loss of a spur gear pair have been determined through testing using the NASA Glenn Research Center Gear Windage Test Facility. The results from this testing have been compared to theoretical results using the formulations presented in this study. Good correlation exist between the test pumping power loss and the predicted pumping power loss for tightly conforming axial shroud configurations.

NOTATION

A_{b1}, A_{b2}	Backlash areas, in^2 (m^2).
A_s	Shroud clearance area, in^2 (m^2).
b	Face width, in (m).
C_d	Discharge coefficient.
D_h	Hydraulic diameter, in (m).
F_1, F_2	Pressure tap correction factors.
F_s	Force acting on shroud clearance area A_s, lb$_f$ (N).
l_s	Length of the line of contact at the start of contact, in (m).
P	Wetted perimeter used in Reynolds number, in (m).
P_p	Pumping power loss ft lb$_f$ (N m).
Q_{max}	Maximum flow rate, in^3/s (m^3/s).
Q_{mean}	Mean flow rate, in^3/s (m^3/s).
Q_{min}	Minimum flow rate, in^3/s (m^3/s).
Re_{Dh}	Reynolds number based on hydraulic diameter.
r_{a1}, r_{a2}	Addendum radii of the drive, driven gear, in (m).
r_{p1}, r_{p2}	Pitch radii of the drive, driven gear, in (m).
w_1, w_2	Orifice width, approach width in (m).
v_s	Velocity through shroud clearance area in/s (m/s).
x	Volume ratio of air to air-oil mixture.
α	Pressure angle of gear set, radians.
β	Ratio of orifice diameter to approach diameter.
ω_1	Angular velocity of the drive gear, rad/s.
ρ	Density of air-oil mixture lb$_m$/in^3 (kg/m^3).
ν	Kinematic viscosity, ft^2/s (m^2/s).

INTRODUCTION

High speed rotorcraft transmissions are subject to load-independent power losses. The load-independent losses associated with high speed rotorcraft transmissions can easily approach 2-3% of the turbine engine transmitted power [1]. In addition, these losses introduce significant implications for onboard oil cooling requirements, lube system capacity, available mission range and standby military readiness for rotorcraft and carrier-based aircraft. Load-independent losses of gear sets consist of drag loss and pumping loss [2]. This study will develop a swept volume approach to calculating the pumping loss of gear pairs. An accounting of pumping loss and drag loss for a spur gear pair tested at the NASA Glenn Research Center (GRC) Gear Windage Test Facility will be compared to predicted pumping loss using the formulations presented in this study.

The term windage was used in the literature initially to describe the drag loss of gears and gear sets and was borrowed

Presented at the Vertical Flight Society's 75th Annual Forum & Technology Display, Philadelphia, PA, USA, May 13-16, 2019.

from the work done on gas turbine disk losses [3]. Oxford Dictionary defines windage as the air resistance of a moving object, such as a vessel or a rotating machine part, or the force of the wind on a stationary object. Pocketing loss, jetting loss, or trapping and squeezing loss have been lumped into windage loss implying a drag characteristic to these losses. However, for tightly shrouded gears, these types of losses are driven by the displacement, or swept volume, resulting from the meshing action of the rotating gear set. The concept of swept volume is used in pump and compressor design to quantify the capacity of the device, but can also be instructive in tightly shrouded gearbox design to quantify potential pumping loss of the transmission.

Losses in geared systems can be divided into load-dependent and load-independent losses. Load-dependent losses are losses incurred in the gears and bearings that increase proportionally with applied load. Load-independent losses, or spin-losses, as described by Kahraman and others [4], are those losses incurred without an applied load. Gear load-independent losses include losses resulting from (1) viscous drag on the faces of the gear; (2) impingement of the air and oil medium on the gear teeth, also known as pressure torque [5]; and (3) pumping of the air and oil medium as mating gear teeth proceed through mesh. High velocity jetting is believed to occur during the "engaging" portion of the mesh cycle for a pair of spur gear teeth in mesh. In general, gear load-independent losses have been found to significantly affect gearbox efficiency above 10,000 ft/min pitch-line velocity [6], [7].

Researchers have determined that the use of shrouding can mitigate viscous and pressure torque drag losses. For meshed spur gears, shrouding involves enclosing the components axially and radially with strategically placed drain holes. Hill [5] demonstrates through computational fluid dynamics (CFD) analysis of a single shrouded spur gear that shrouding acts to preserve the fluid velocity in the vicinity of a rotating gear, resulting in reduced power consumption. In general, the load-independent losses are reduced with decreasing axial and radial clearance between the stationary shroud and the rotating gear. However, recent results from tests conducted on shrouded meshed spur gears by Delgado and Hurrell [8] show that the beneficial effects of shrouding may be offset by pumping loss in the vicinity of the gear mesh.

Power loss results from the NASA experiments for different shroud configurations for a pair of meshed spur gears is reproduced in Figure 1. The experiments were conducted at NASA GRC Windage Test Facility. From previous research using single shrouded spur gears, the small axial, small radial clearance configuration results in the largest reduction in power loss [9]. However, the largest reduction in load-independent losses from experiments conducted using shrouded meshed spur gears are realized using the large axial, small radial clearance shroud configuration. The small axial, small radial clearance configuration exhibits a larger than expected total loss which is attributed to a larger pumping power loss. The close clearance axial shrouds act to redirect the flow resulting from the meshing action of the gear set. The resulting flow is redirected back toward the gear faces and through the backlash clearances and the tight shroud clearances.

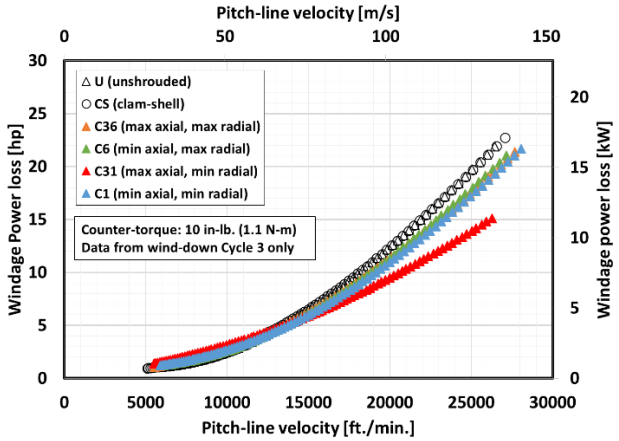

Figure 1 Comparison of meshed spur gear load-independent power loss versus shroud configuration clearances for wind-down cycle 3.

The pumping action of meshed gears has been studied by several researchers. Early acoustic experiments by Rosen [10] indicate that as gear teeth proceed through mesh the fluid is forced out of the space between the mating gear teeth. Dudley [11] notes that air and lubrication oil may become trapped in the mesh region, resulting in power loss, and "to allow for plenty of room within the casing" to possibly mitigate this effect. Wittbrodt and Pechersky [12] describe the phenomenon as the air and lubricant in the volume space between mating teeth being compressed and forced out of the "sides" and "between" the mating teeth. Diab et al. [13] describe the phenomenon as a trapping of the air and oil mixture in the tooth interspaces. The trapped volume undergoes a compression and expansion within a mesh cycle. The air-oil mixture can flow in both the axial and radial directions. Seetharaman and Kahraman [14] describe the phenomenon as "pocketing," where the air and oil mixture is treated as a compressible fluid confined by the cavity making up a tooth on one gear and the mating space between two adjacent teeth on the opposing gear, or inter-tooth space. As a result of the meshing of mating gear teeth, the volume of air and oil is squeezed, resulting in a higher-pressure inside the trapped volume with respect to outside the volume. The mixture is forced out of the ends and backlash regions of the inter-tooth cavity.

Past studies have been conducted to model the power loss due to oil "trapping" and "acceleration" [15]. Wittbrodt and Pechersky [12] perform a one-dimensional incompressible and compressible flow analysis that shows higher fluid flow at the gear tooth tips compared to axial flow at the ends of the gear teeth. Fluid velocities may reach sonic conditions and are dependent on rotational speed and the relative gear

geometries. Peak velocities are shown to occur prior to the gear teeth reaching the pitch point in the mesh cycle. The position of maximum velocity varies with gear geometry. Regarding the specific rotational position of maximum end flow, positive or negative, Wittbrodt and Pechersky's analysis provides a number of factors that affect this location. Higher pitch-line velocities, smaller backlash, and a larger gear ratio tend to move the maximum velocity earlier in the mesh cycle. One particularly interesting result indicates that the tooth space velocity approaches zero just after the pitch point. Rosen's work shows that the fluid velocities exiting the tooth space become negative after the pitch point, indicating a reversal in fluid flow from expulsion to ingestion [10]. While Wittbrodt and Pechersky do not explicitly discuss this, several other researchers [10], [13], [14] report negative fluid velocities after the meshing spur gears pass the pitch point (i.e., fluid ingestion into the gear tooth spaces).

Using conservation of momentum principles, Seetharaman and Kahraman [14] calculate discharge velocities at the ends and backlash regions of mating spur gear teeth. Analyses show a maximum positive velocity (i.e., expulsion) prior to the pitch point and a maximum negative velocity (i.e., suction) after the pitch point. The absolute magnitude of these velocities increases with increasing pitch-line velocity. For the unity ratio gears analyzed, end-flow pressures increase with increasing pitch-line velocity. End-flow pressure magnitudes are slightly less than the magnitudes of the backlash pressure. Correspondingly, end-flow velocities are slightly lower than backlash flow velocities for a given rotational position.

Al et al. [16] perform a single-phase two-dimensional modeling study of meshed spur gears. The mesh between the gear teeth is modeled as the teeth proceed through the mesh cycle. Contact between the gear teeth is not modeled and axial flows are not considered. Results support the existence of a maximum positive pressure prior to the mesh pitch point. The results also support the observation of other researchers that a period of expulsion (positive flow) exists prior to the mesh pitch point, followed by a period of suction (negative flow) after the mesh pitch point. The results are in agreement with experimental data by Diab et al. [13]. Burberi et al. [17] simulate meshed spur gears rotating in a submerged oil with the flow modeled as an isothermal and incompressible fluid. A dynamic mesh, moving boundary approach is used with the gear teeth not in contact. The results show oil flow moving out of and into mesh.

Particle image velocimetry (PIV) studies by Hartono et al. [18], [19] for unshrouded meshed spur gears at different levels of oil immersion show recirculation of fluid flow that impinges on the sides and faces of the gear teeth. Pitch-line velocities were limited to less than 20 m/s (3,937 ft/min). Visual analysis in a fully immersed condition at 0.55 m/s (108 ft/min) and 1.1 m/s (217 ft/min) gear pitch-line velocity indicate fluid movement into mesh. The particle trajectories, or streamlines, as the mating gear teeth enter the mesh zone show an axially outward flow that increases in intensity with pitch-line velocity.

The use of computational fluid dynamic (CFD) methods has recently been applied to model gear transmission load-independent losses [20], [21], [22] [23], [24]. Modeling of two gears meshing is difficult because of the collapse and expansion of the tooth space volumes during the mesh cycle. Incorporating other details in the model such as two-phase flow and shroud effects further complicates the analysis.

TEST FACILITY

The load-independent loss tests presented in this study were conducted using the NASA GRC Gear Windage Test Facility. A sketch of the facility test rig is shown in Figure 2. The rig is driven by a 150 horsepower (112 kW) DC drive motor that is connected to a 5.17:1 ratio speed-up gearbox. The output of the speed-up gearbox is connected to a torque meter which in turn is connected to a hydraulically actuated clutch and the input shaft to the test gearbox through flexible couplings. The output shaft of the test gearbox is connected through another hydraulically actuated clutch and flexible couplings to an eddy current dynamometer (magnetic particle brake) that can provide load to the test gear set.

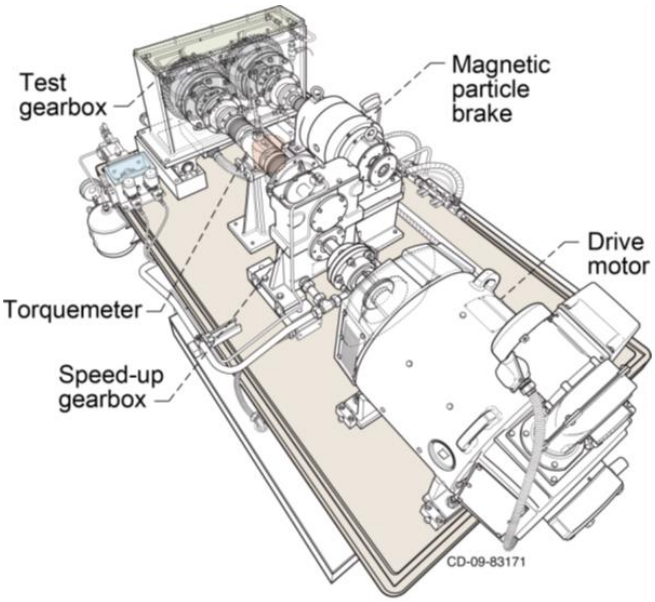

Figure 2 Overview sketch of the NASA Glenn Research Center Gear Windage Rig.

Speed sensors consisting of 60-tooth wheels are mounted on the rig shafting. For each speed wheel a variable reluctance magnetic speed sensor is bracket-mounted to the rig frame to measure shaft speed. The facility has five speed wheel and magnetic speed sensor pairs located at the drive motor, speed-up gearbox input shaft, test gearbox input shaft, test gearbox output shaft, and the dynamometer. Accelerometers are located at the speed-up gearbox, torque meter, test gearbox, and dynamometer. Thermocouples are located at the oil inlet and oil exit of the test gearbox, at the two bearing locations

supporting the test gearbox input shaft and the two bearing locations supporting the test gearbox output shaft, and at a location just out-of-mesh of the test gears to measure gear fling-off temperature. The gear-fling off temperature is measured at the 1 o'clock position, or 30 degrees clockwise from the vertical, on the drive side test gear. Torque is measured with a rotary torque sensor rated at 2000 in.-lb. (226 Nm) and located in-line between the speed-up gearbox and test gearbox prior to the hydraulically actuated clutch on the test gearbox drive shaft.

The test gearbox can accommodate either single, or meshed, spur gears corresponding to the single, or dual shaft, modes of operation. The input and output shafts both have hydraulically actuated clutches that allow the test gearbox in single, or dual shaft mode, to be disconnected from the motor and the dynamometer and the test gear(s) and shaft(s) to coast down from an initial speed to zero speed. During a typical test, the free spin down of the test article(s) is used to measure the loss of the test configuration. Gear lubrication is provided during single and dual mode operation of the test rig at a rate of 0.62 gpm (2.3 lpm). The temperature of the lubrication oil and shroud interior is allowed to reach 100°F (38°C) and stabilize prior to the start of each test. The position of the two lubrication jets and the rotation of the gear set during dual mode rig operation provide lubrication into-mesh. Out-of-mesh jet lubrication is not used during dual mode operation of the NASA GRC gear windage rig.

Gear mesh load during the free spin down is mainly a result of the resistive torque of the load-independent loss, i.e., spin down loss. The torque resulting from the spin down loss, typically between 10 to 15 in-lbs. (1.1 to 1.7 Nm), can be used to calculate the sliding and rolling power losses of the test gear set. The resulting sliding and rolling power loss is two orders of magnitude smaller than the spin down power loss typical of a spin down test conducted on the NASA gear windage rig. Therefore, the mesh losses due to sliding and rolling are considered insignificant compared to the overall spin down power loss.

A sketch of the test gearbox showing the major components of the gear shroud support structure contained within the gearbox is shown in Figure 3. The test gearbox interior dimensions are approximately 6 inches (0.15m) wide by 16 inches (0.41m) deep by 28 inches (0.71m) high. The test gears can be run in the gearbox with, or without, shrouding. The shrouding clearance can be adjusted radially and axially as shown in Figure 4 and Figure 5. Aluminum plates 1/4-inch-thick (6.35 mm) are used for the axial shrouds while 1/16-inch-thick (1.5875 mm) low-carbon steel sheet metal strips are used for the radial shrouds. The shrouds are contained within, and held in place by, the clam-shell housing which in turn is bolted to the gearbox structure. The shroud surface roughness is approximately 63 micro-inches (1.6 micro-meter). Six machined axial slots within the clam-shell housing allow for set clearances between the axial shroud wall and the test gear as seen in Figure 5. The axial shroud walls, in turn, have six machined radial slots to vary the radial shroud position, Figure 4. For ease of assembly, the clam-shell housing is composed of four pieces: 1) upper drive-side; 2) lower drive-side; 3) upper driven-side; 4) lower driven-side. The entire assembly is bolted within the test gearbox as shown in Figure 3.

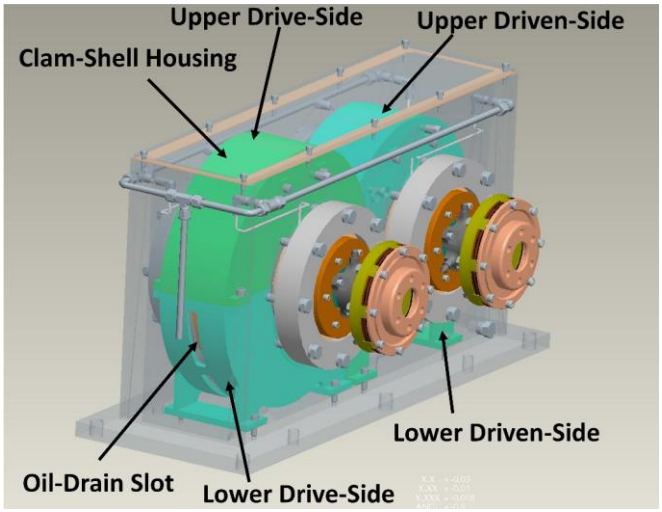

Figure 3 Test gearbox showing clam-shell enclosure for shrouding within the NASA Gearbox.

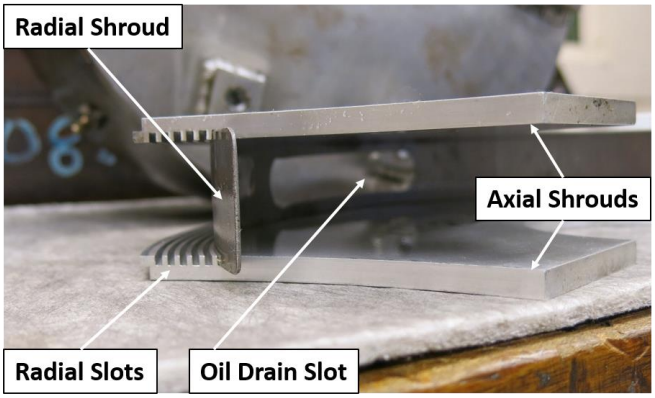

Figure 4 Configuration of radial and axial shrouding. Axial shrouds are 1/4 in. (6.35 mm) thick and radial shrouds are 1/16 in. (1.5875 mm) thick.

Figure 5 Configuration of axial and radial shrouding using machined slots.

Figure 6 illustrates the radial shrouds assembled in the back half of the axial shrouds. The top joint of the figure eight formed by the radial shrouds contains a clearance gap and is shown in a close-up view in Figure 7. The clearance gap defines the shroud clearance area through which the swept volume flow is forced to exit the shroud structure.

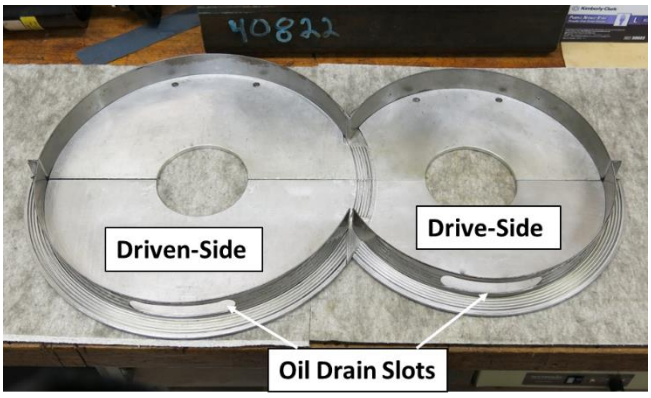

Figure 6 Radial shrouds installed in back half of the axial shrouds.

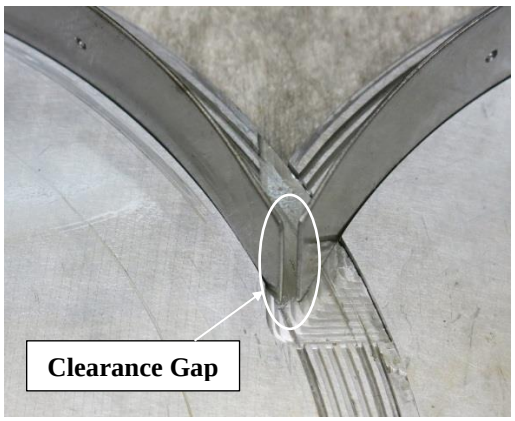

Figure 7 Radial shroud clearance gap.

The spur gears used in this study are shown in Figure 8 and the pertinent gear parameters are given in Table 1.

Figure 8 Test spur gears.

Gear Parameter	Drive-side	Driven-side
number of teeth	44	52
pitch/mod., 1/in (mm)	4 (6.35)	
face width, in (mm)	1.12 (28.4)	1.12 (28.4)
pitch dia., in (mm)	11.0	13.0 (330.2)
pressure angle, deg (rad)	25 (0.44)	
outside dia., in (mm)	11.49	13.49
Material	Steel-SAE 5150H	
surface finish, µin (µm)	16 (0.4)	

Table 1 Spur gear pinion (drive-side) and gear (driven-side) specifications.

SWEPT VOLUME DERIVATION

The literature indicates many similarities in flow patterns between meshing transmission gears and positive displacement pumps, or compressors. Strong outflow (discharge) and inflow currents (suction) have been observed by many of the studies of gear transmissions as the gears proceed into and out of mesh. Shrouding of transmission gears with tightly conforming axial and radial shrouds change the flow patterns around the gear set. The bulk flow resulting from the pumping action of a shrouded gear set is similar to the swept volume flow of an external gear positive displacement pump. The flow within a gear pump is depicted in Figure 9. A gear pump typically has tight radial clearance between the gear and housing. In addition, tight axial clearances typically exist between the gear faces and the two pump end plates. The tight clearances are to reduce leakage from the high pressure discharge to the low pressure inlet. Blocking, or restricting, the discharge of a positive displacement pump increases the upstream pressure and the required drive torque of the pump forcing a higher percentage of the total flow through leak paths back to inlet. In a shrouded gear set, the main paths for the leakage flow are

through the backlash spacing between the tooth pairs going into mesh and the clearance spaces of the shroud design.

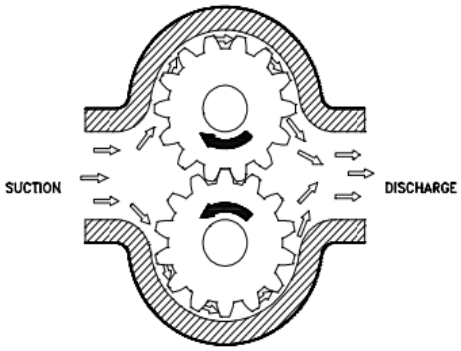

Figure 9 Flow within an external gear positive displacement pump.

For the tightly shrouded NASA GRC spur gear set, it is reasonable to assume that the majority of the swept volume flow discharges through the radial shroud clearance gap. The progression of the volume of air-oil mixture carried by the tooth spaces is shown in Figure 10. The blue colored volumes represent the swept volume of the tooth space prior to entering the mesh zone. A similar set of volumes depicted as green and yellow are entering the mesh zone. The fluid contained in these volumes is being squeezed and forced through the two tooth space ends and the backlash areas of the respective volumes. The last set of volumes shown as red are trapped between the two points of contact (lines into the page) and the fluid contained in these volumes is prevented from escaping through the backlash areas subsequently forcing the fluid axially through the end areas of the collapsing volumes.

Consider the shrouded transmission gear set as a pump, or compressor, with the discharge area A_s as shown in Figure 10. This is representative of the shroud configuration tested at NASA GRC. The swept volume, or displacement, of the gear set is the volume of fluid carried by the tooth spaces of the two gears per one revolution of the drive gear. The radial shroud clearance dictates the size of the discharge area and as the clearance decreases, the restriction to the discharge flow increases. The pumping losses of the gear set are related to the swept volume of the gear tooth spaces and the leakage path that the volume of fluid is forced to traverse to exit the shroud structure.

Prior to tooth contact, the swept volume is forced axially out the ends of the tooth spaces and through the area created by the backlash of the gear pair as the tooth space volume collapses. Once tooth contact is made, a portion of the swept volume is trapped between the meshing gear teeth, squeezed, and jetted out of the tooth space ends in the axial direction. This jetted flow, along with the remaining swept volume not carried through the gear mesh, is forced through the shroud clearance to the gear box drain. During this whole process, the flow restriction is a combination of the total flow path at any instant which includes flow through the shroud clearance area A_s, flow through the backlash areas A_{b1}, A_{b2} and axial flow through the ends of the collapsing tooth spaces.

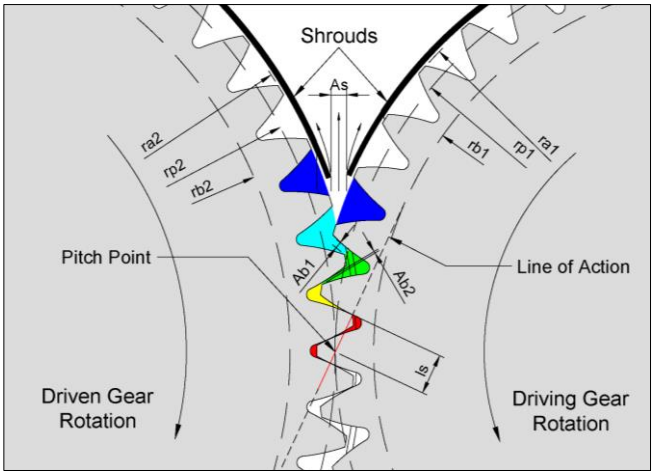

Figure 10 Shrouded gear pair proceeding through mesh.

Manring and Kasaragadda [25] develop a relation for the maximum flow rate of a gear pump based on the swept volume of the mating gears. Applying these relations to a shrouded gear pair, the maximum flow rate Q_{max} is a function of the face width b, addendum radii of the drive and driven gears r_{a1}, r_{a2}, the pitch radii of the drive and driven gears r_{p1}, r_{p2} and the angular velocity of the drive gear ω_1.

$$Q_{max} = \frac{b\omega_1}{2}\left[r_{a1}^2 + r_{a2}^2\frac{r_{p1}}{r_{p2}} - r_{p1}(r_{p1} + r_{p2})\right] \quad (1)$$

A similar relationship for the minimum flow rate was developed

$$Q_{min} = \frac{b\omega_1}{2}\left[r_{a1}^2 + r_{a2}^2\frac{r_{p1}}{r_{p2}} - r_{p1}(r_{p1} + r_{p2}) - \left(1 - \frac{r_{p1}}{r_{p2}}\right)l_s^2\right] \quad (2)$$

where l_s, shown in Figure 3, is the length of the line of contact at the start of contact and is calculated, knowing the pressure angle of the gear set α, using the following equation [25].

$$l_s = \sqrt{r_{a2}^2 - r_{p2}^2(\cos\alpha)^2} - r_{p2}\sin\alpha \quad (3)$$

Note that the swept volume flow fluctuates periodically with the mesh frequency of the gear set. The amplitude of the swept volume flow is the difference between the maximum and minimum flow rates and corresponds to the amount of flow decrement due to the trapped volume created by the contacting gear teeth. The trapped volume is carried through mesh to the disengaging side of the pitch point and to the lower pressure side of the shroud enclosure. Subsequently, the mean flow rate is given as the sum of the amplitude of the swept volume flow rate and the minimum swept volume flow rate.

$$Q_{mean} = \frac{Q_{max} - Q_{min}}{2} + Q_{min} \quad (4)$$

The velocity of air and oil mixture through the shroud clearance area A_s can be approximated assuming steady

uniform incompressible flow using the mean flow rate and a discharge coefficient C_d.

$$v_s = C_d \frac{Q_{mean}}{A_s} \quad (5)$$

A discharge coefficient for a sharp-edged orifice is used in this study to approximate flow through A_s. The ISO-ASME Orifice Coefficient Equation [26] relates the discharge coefficient for a given ratio of orifice diameter to approach diameter as a function of Reynolds number. The equation is used in this study to obtain a discharge coefficient as a function of Reynolds number since the Reynolds number varies continuously with the surface speed of the gear set. Since the orifice and approach areas are rectangular in shape, then characteristic widths are used instead of diameters. Defining the ratio of widths as

$$\beta = \frac{w_1}{w_2} \quad (6)$$

where w_1 is the orifice width and w_2 is the approach width.

The discharge coefficient is defined as

$$C_d = f(\beta) + 91.71\beta^{2.5} {Re_{Dh}}^{-0.75} + \frac{0.09\beta^4}{1-\beta^4} F_1 - 0.0337\beta^3 F_2 \quad (7)$$

where

$$f(\beta) = 0.5959 + 0.0312\beta^{2.1} - 0.184\beta^8 \quad (8)$$

The ISO-ASME Orifice Coefficient Equation contains pressure tap correction factors for orifice upstream and downstream pressure measurements. For this study, radius type taps were chosen for the curve fit where $F_1 = 0.4333$ and $F_2 = 0.47$ [26]. A Reynolds number based on a hydraulic diameter is used given that the orifice area is rectangular instead of circular.

$$Re_{Dh} = \frac{4Q_{mean}}{\pi D_h \nu} \quad (9)$$

where

$$D_h = \frac{4A_s}{P} \quad (10)$$

ν is the kinematic viscosity of the air-oil mixture and P is the wetted perimeter. The shroud clearance area A_s is calculated as the product of the approach width w_2 and the axial distance between the two axial shrouds l_a.

$$A_s = w_2 l_a \quad (11)$$

Likewise, the wetted perimeter is the sum of the approach width w_2 and the axial distance between the two axial shrouds l_a.

$$P = w_1 + l_a \quad (12)$$

The force of fluid F_s acting on the shroud clearance area can be approximated knowing the density of the air-oil mixture ρ.

$$F_s = \rho v_s^2 A_s \quad (13)$$

The density of the air-oil mixture is approximated using the percent volume for each component of the mixture present during the NASA GRC tests. Defining the volume ratio of air to oil-air mixture x.

$$x = \frac{Q_{air} - Q_{lube}}{Q_{total}} \quad (14)$$

Then the density of the mixture is estimated as

$$\rho = x\rho_{air} + (1-x)\rho_{oil} \quad (15)$$

Similarly, the kinematic viscosity of the air-oil mixture ν is estimated based on percent volume.

The pumping power loss P_p due to the forced discharge of swept volume flow through the shroud clearance area is then the product of the force of fluid acting on this area and the velocity of the fluid through the area.

$$P_p = F_s v_s \quad (16)$$

RESULTS

Drag for the two test gears run in single mode operation of the test rig using closely conforming shrouds is shown in Figure 11 along with a total drag for the gear set. The shroud clearance for the single gear tests are 0.039 inch (0.991 mm) radially and 0.039 inch (0.991 mm) axially. Total drag for the two test gears is determined as the sum of drag from the single mode tests.

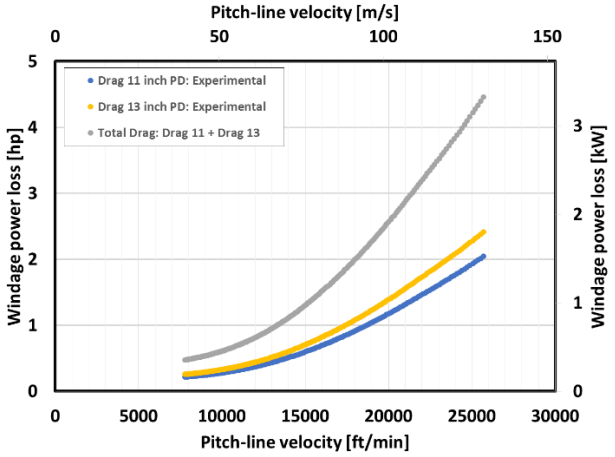

Figure 11 Experimental drag loss for single gears tested in C1 (min axial, min radial) shroud configuration.

Figure 12 shows the C1 shroud configuration with the meshing gears and a minimum radial shroud clearance of 0.039 inch (0.991 mm). Also shown is the clearance gap between the two top radial shrouds of 0.214 inch (5.44 mm). The C1 shroud configuration provides a minimum axial (not shown) and radial shroud clearance of 0.039 inch (0.991 mm).

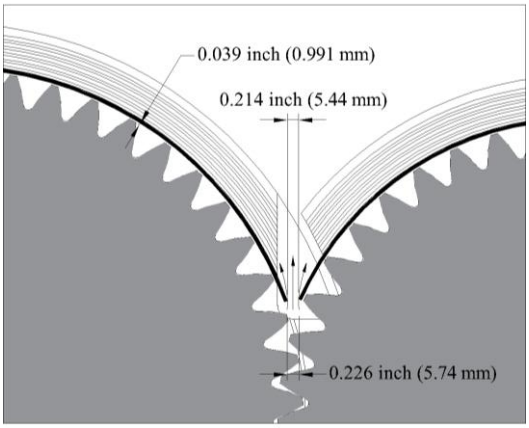

Figure 12 C1 (min axial, min radial) shroud configuration showing shroud clearance gap.

Test results for total load-independent losses for the meshed spur gear set operated in dual mode operation of the test rig with the C1 shroud configuration are shown in Figure 13. Also shown is the total drag of the two gears determined from single mode testing of the individual gears. The pumping loss shown is the difference between the total load-independent loss of the meshed gears and the total drag. Also shown is the predicted pumping power loss for the shrouded gear set using the swept volume calculations presented earlier. The predicted pumping power loss is determined using the top radial shroud clearance gap shown in Figure 12. Density and viscosity of the air-oil mixture used in the pumping power loss calculations are estimated based on the percent volume formulation for a temperature of 100°F (38°C) at atmospheric pressure.

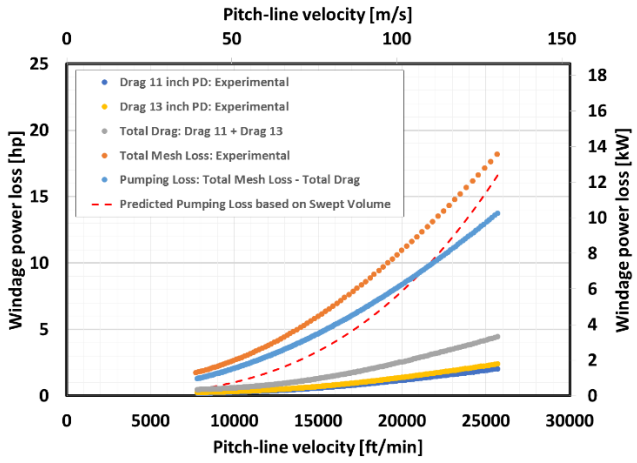

Figure 13 Load-independent loss breakdown for meshed gears in C1 (min axial, min radial) shroud configuration.

In order to test the applicability of the swept volume prediction, the same formulations are applied to a different shroud configuration. The C6 shroud configuration with meshing gears and a maximum radial shroud clearance of 0.660 inch (16.8 mm) is shown in Figure 14. The clearance gap between the two top radial shrouds for this configuration is 0.154 inch (3.91 mm) as shown in the figure. The C6 shroud configuration provides a minimum axial (not shown) shroud clearance of 0.039 inch (.991 mm), and a maximum radial shroud clearance of 0.660 inch (16.8 mm).

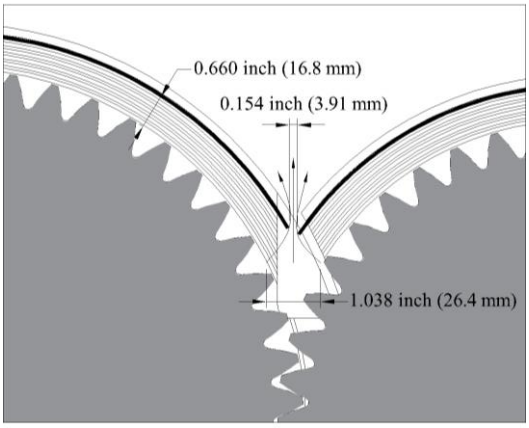

Figure 14 C6 (min axial, max radial) shroud configuration showing shroud clearance gap.

Test results for the load-independent losses for the meshed gear set operated in dual mode operation of the test rig with the C6 shroud configuration are shown in Figure 15. Also shown is the total drag of the two gears determined from the single mode testing of the individual gears. Once again, the pumping loss shown is the difference between the total load-independent loss of the meshed gears and the total drag. The predicted pumping loss for the shrouded gear set using the swept volume calculations presented earlier is also shown. The shroud clearance area A_s, is determined using the top radial shroud clearance gap shown in Figure 14. Once again, density and viscosity of the air-oil mixture used in the pumping power loss calculations are estimated based on the percent volume formulation for a temperature of 100°F (38°C) at atmospheric pressure.

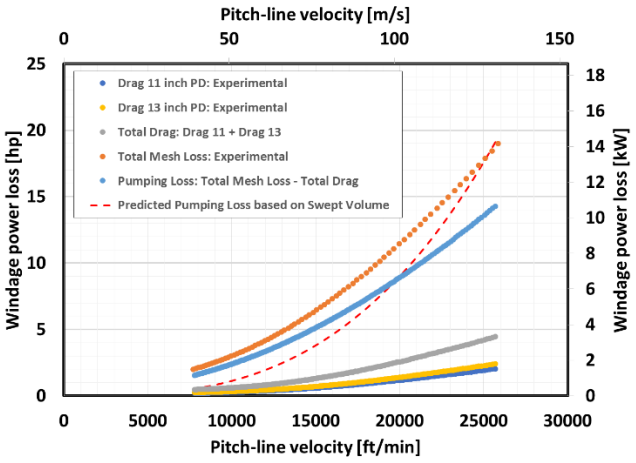

Figure 15 Load-independent loss breakdown for meshed gears in C6 (min axial, max radial) shroud configuration.

CONCLUSIONS

An accounting of pumping loss and drag loss for a shrouded spur gear pair tested at the NASA GRC Gear Windage Test Facility has been used for comparison to predicted pumping loss for the tested configurations. The pumping loss estimation is based on the swept volume formulation presented in this study. Estimation of pumping loss based on the gear pair swept volume was determined for two of the shroud configurations tested. From the test results, pumping loss is seen to be a significant portion of the total load-independent loss at pitch-line velocities in excess of 25,000 ft/min (127 m/s). For high speed rotorcraft transmissions, an estimate of pumping loss is critical for determining the overall load-independent loss of the system.

Comparing the pumping loss determined from tests conducted on the NASA GRC windage test facility and the predicted pumping loss determined using the swept volume formulations indicate the prediction is best for closely conforming shrouds. However, the predicted pumping loss deviates from actual when the shroud clearances are increased from the minimum. The large radial clearances provided by the C6 positioning of the radial shrouds allows for a larger portion of the swept volume flow to bypass the shroud clearance area A_s. As a result, the swept volume prediction of pumping loss, which assumes all of the swept volume flow is discharged through A_s, over-estimates the pumping power loss significantly at high pitch-line velocities. Similar results are seen for shroud configurations with large radial clearances.

The flow pattern of a set of shrouded spur gears with tight shroud clearances closely resembles the flow pattern of a gear pump. However, as the clearances grow from the minimum, more of the swept volume flow leaks past the rotating gears and less flow is discharge through the shroud clearance area A_s. The flow pattern for a set of shrouded gears enclosed in shrouds with a large radial and/or a large axial clearance deviates from that of an external gear pump. Therefore, the applicability of the swept volume prediction is limited to gear sets enclosed within tight radial and axial clearance shrouds with a well-defined flow discharge area.

The interaction between pumping loss and shroud configuration for a pair of shrouded spur gears is highlighted in this study. Given that the swept volume (displacement) is the same for a set of gears, then the pumping losses are throttled down, or up, depending on the shroud configuration and clearance path restrictions. Based on these observations, one method of reducing pumping loss of tightly shrouded gear sets, is to provide sufficient shroud clearance area for the swept volume flow to be discharged out of the shroud structure to gearbox drain. Dudley [11] had a similar observation back in 1962.

The swept volume formulation also highlights the relationship between pumping loss and gear geometry. Based on the swept volume formulation, pumping loss increases as gear pitch decreases, face width increases, and pitch-line velocity increases. For a given application, studies with the objective of reducing pumping power loss can be conducted varying these gear parameters along with a low pumping loss shroud configuration.

Author contact: Michael Hurrell michael.j.hurrell@nasa.gov, Irebert Delgado irebert.r.delgado@nasa.gov, Jerzy Sawicki j.sawicki@csu.edu.

ACKNOWLEDGMENTS

The authors acknowledge the support of the NASA Revolutionary Vertical Lift Technology Project and also to Sigurds Lauge (HX5 Sierra LLC) for technical test support.

REFERENCES

1. Handschuh, R., and Kilmain, C., 2006, Operational Influence on Thermal Behavior of High-Speed Helical Gear Trains. AHS International 62nd Annual Forum and Technology Display, Phoenix, Arizona.
2. Seetharaman, S., Kahraman, A., 2010, "A windage power loss model for spur gear pairs," Tribology Transactions, 53(4), pp.473–484.
3. Townsend, D. : Dudley's Gear Handbook, 2nd Edition, McGraw-Hill, Inc., 1992.
4. Kahraman, A., D. R. Hilty, and A. Singh. "An experimental investigation of spin power losses of a planetary gear set." Mechanism and Machine Theory 86 (2015): 48-61.
5. Hill, M.J., 2010, "A Computational Investigation of Gear Windage." Ph.D. thesis, The Pennsylvania State University.
6. Dudley, D. W., Dudley's Gear Handbook. Ed. Dennis P. Townsend. Tata McGraw-Hill Education, 1991, 12.24.
7. Diab, Y., Ville, F., Velex, P. and Changent, C.: "Windage Losses in High Speed Gears – Preliminary Experimental and Theoretical Results." Journal of Mechanical Design, Vol. 126, Sept. 2004, pp. 903 – 908.
8. Delgado, I., and Hurrell, M., 2017, "The Effectiveness of Shrouding on Reducing Meshed Spur Gear Power Loss – Test Results." AGMA Fall Technical Meeting, Columbus, Ohio.
9. Handschuh, R. F., and Hurrell, M. J., "Initial Experiments of High-Speed Drive System Windage Losses." International Conference on Gears, Munich Germany, Oct. 2010.
10. Rosen MW. "Noises of Two Spur-Gear Transmissions." Noise Control. 1961 Nov; 7(6):11-9.
11. Dudley, D.W., 1962, Gear handbook: the design, manufacture, and application of gears, McGraw Hill Book Company, New York, Chap. 14.

12. Wittbrodt MJ, Pechersky MJ. “A hydrodynamic analysis of fluid flow between meshing spur gear teeth.” Pennsylvania State University, University Park Applied Research Laboratory; 1987 Oct.

13. Diab, Y., Ville, F., Houjoh, H., Sainsot, P., Velex, P. “Experimental and numerical investigations on the air-pumping phenomenon in high-speed spur and helical gears.” Proceedings of the Institution of Mechanical Engineers, Part C: Journal of Mechanical Engineering Science. 2005 Aug 1;219(8):785-800.

14. Seetharaman, S., Kahraman, A., 2010, “A windage power loss model for spur gear pairs.” Tribology Transactions, 53(4), pp.473–484.

15. Ariura, Yasutsune, et al. “The lubricant churning loss in spur gear systems.” Bulletin of JSME 16.95 (1973): 881-892.

16. Al, B.C., Simmons, K., Morvan, H.P. “Computational investigation of flows and pressure fields associated with spur gear meshing.” ASME Turbo Expo 2014: Turbine Technical Conference and Exposition 2014 Jun 16 (pp. V05CT16A023-V05CT16A023). American Society of Mechanical Engineers.

17. Burberi, E., Fondelli, T., Andreini, A., Facchini, B., Cipolla, L. “CFD Simulations of a Meshing Gear Pair.” ASME Turbo Expo 2016: Turbomachinery Technical Conference and Exposition 2016 Jun 13 (pp. V05AT15A024-V05AT15A024). American Society of Mechanical Engineers.

18. Hartono, E., Golubev, M., & Chernoray, V. (2013). “PIV Study of Fluid Flow Inside A Gearbox.” 10th International Symposium on Particle Image Velocimetry, Delft, The Netherlands, July 1-3, 2013.

19. Hartono, E. A., Pavlenko, A., & Chernoray, V. (2014). “Stereo-PIV Study of Oil Flow Inside a Model Gearbox.” 17th International Symposium on Applications of Laser Techniques to Fluid Mechanics (pp. 07-10).

20. Al-Shibl, K., Simmons, K., and Eastwick, C.: “Modeling Windage Power Loss from an Enclosed Spur Gear.” Journal of Power and Energy, Vol. 221, 2007, pp331-341, Proc. IMechE Part A.

21. Marchesse, Y., Changenet, C., Ville, F. and Velex, P.: “Investigations on CFD Simulation for Prediction Windage Power Losses in Spur Gears.” 3rd International Conference on Integrity, Reliability and Failure, Porto, Portugal, July 2009.

22. Imai, H., Goi, T., Arisawa, H., and Nishmimura, M.: “Reduction in Gear Windage and Churning Loss by Optimum Shroud Design with Aid of CFD.” JSME International Conference on Motion and Power Transmission, JSME, Matsushima Isles Resort, Japan, May 2009.

23. Hill, M., Kunz, R., Noack, R., Long, L, Morris, P., and Handschuh, R.: “Application and Validation of Unstructured Overset CFD Technology for Rotorcraft Gearbox Windage Aerodynamics Simulation.” AHS Forum 64, Montreal, Canada, April 2008.

24. Hill, M. J., Kunz, R. F., Medvitz, R. B., Handschuh, R. F., Long, L. N., Noack, R. W., and Morris, P. J., “CFD analysis of gear windage losses: Validation and parametric aerodynamic studies.” Journal of Fluids Engineering, Vol. 133, (3), Mar. 2011, 031103.

25. Manring, N. D., Kasaragadda, S. B. The Theoretical Flow Ripple of an External Gear Pump. Transactions of ASME, Vol. 125, Sept. 2003.

26. ASME Fluid Meters Research Committee, The ISO-ASME Orifice Coefficient Equation, Mech. Eng. July 1981, pp. 44-45.